ACS APPLIED MATERIALS & INTERFACES

Research Article

www.acsami.org

Highly Reversible Li Storage in Hybrid NiO/Ni/Graphene Nanocomposites Prepared by an Electrical Wire Explosion Process

Duk-Hee Lee, Jae-Chan Kim, Hyun-Woo Shim, and Dong-Wan Kim*

Department of Energy Systems Research and Department of Materials Science and Engineering, Ajou University, Suwon 443-749, Korea

Supporting Information

ABSTRACT: NiO/Ni/graphene nanocomposites were prepared using a simple and environmentally friendly method comprising an electrical wire pulse technique in oleic acid containing graphenes and subsequent annealing to form anodes for Li ion batteries. The control product of NiO/Ni nanocomposite was prepared under the same conditions and characterized by structural and electrochemical analysis. The obtained NiO/Ni/graphene nanocomposite particles had sizes of 5−12 nm and a high surface area of 137 m^2 g^{-1}. In comparison to NiO/Ni, NiO/Ni/graphene exhibited improved cycling performance and good rate capability. Reversible capacity was maintained at over 600 mA h g^{-1} at 0.2 C and was attributed to the alleviation in volume change and improved electrical conductivity of NiO/Ni/graphene nanocomposites.

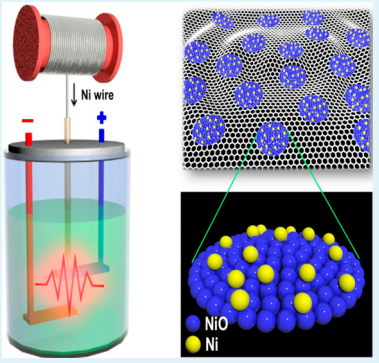

KEYWORDS: *NiO/Ni/graphene, nanocomposites, electrical wire explosion, Li ion battery*

I. INTRODUCTION

Li-ion batteries (LIBs) have found widespread use as power sources in portable electric devices and electric vehicles recently. Significant research into various other applications has also been carried out. Electrode materials form a vital component of LIBs and are finding increasing additional applications. Although graphite has been the preferred choice for the anode material in commercial LIBs, elemental metals (Si, Sn, Ge, Zn, etc.) and transition metal oxides have also been explored due to the relatively low theoretical capacity of graphite (372 mA h g^{-1}).[1−6]

Nanosized transition metal oxides are able to deliver large Li-storage capacity due to the conversion reaction with Li ($M_xO_y + 2yLi \leftrightarrow yLi_2O + xM$, M = Co, Cu, Fe, Ni, etc.) and thus have been extensively studied as potential anode materials.[7−9] Among these metal oxides, NiO is an attractive material due to its high theoretical capacity (718 mA h g^{-1}), which is about 2 times higher than when graphite is used as the anode, abundance, low cost, and environmental safety. Synthesis of nanostructured NiO for use as anode materials that include nanoflakes, nanoparticles, nanotubes, nanosheets, and nanocomposites has been the subject of current studies.[10−15] Several methods were used for the synthesis of nanostructured NiO such as physical and chemical thermal vapor deposition, hydrothermal, and sol−gel process.[16−19] However, transition metal oxides including NiO undergo significant volume change during the repetitive charge−discharge process due to the conversion reaction with lithium ion, causing capacity fading and poor cycling performance.[1,7]

In order to overcome the limitations associated with single-phase nanomaterials, various hybrid nanostructures have recently been proposed.[20−24] A hybrid combination of various nanomaterials is expected to improve energy and power densities of LIBs. A combination of transition metal oxides with carbonaceous materials to fabricate hybrid nanostructured anodes using several techniques have routinely been proposed[25−28] and has proved to be an effective strategy to enhance electron transport. It was discovered in 2004 that graphene with its two-dimensional single layer of graphite displayed good mechanical strength and thermal properties, excellent electric conductivity, and high surface area. Graphene may also deliver other additional properties that surpass graphite and carbon nanotubes leading to improved electrochemical performance in LIBs. Even at a very low weight fraction, graphene can serve as an efficient electron conducting network and an excellent support that acts as a buffer for the volume variation of electrode materials.[29−31] Newer studies have reported the fabrication of NiO/graphene composites that have enhanced electrochemical performance.[32−34]

In this paper, we report the fabrication of hybrid NiO/Ni/graphene nanocomposites by a simple two-step procedure: (1) initial synthesis of Ni nanoparticles on graphenes using a low-cost and scalable electrical wire explosion process in oleic acid (OA) as liquid solvent media containing graphenes, and (2) partial oxidation of Ni in the as-prepared Ni/graphene composites at 300 °C in air. We show that the uniform distribution of NiO/Ni nanoparticles on graphenes allows the achievement of a large surface area and enables electrical

Received: August 28, 2013
Accepted: October 14, 2013
Published: October 14, 2013

   dx.doi.org/10.1021/am403643x | ACS Appl. Mater. Interfaces 2014, 6, 137−142

connection to a current collector through the electrically conducting graphenes networks. Furthermore, we demonstrate the superior electrochemical properties of hybrid NiO/Ni/graphene nanocomposite anodes compared with their NiO/Ni counterparts.

II. RESULTS & DISCUSSION

Figure 1a shows the photograph of the set up for the preparation of nanocolloids during the electrical wire explosion

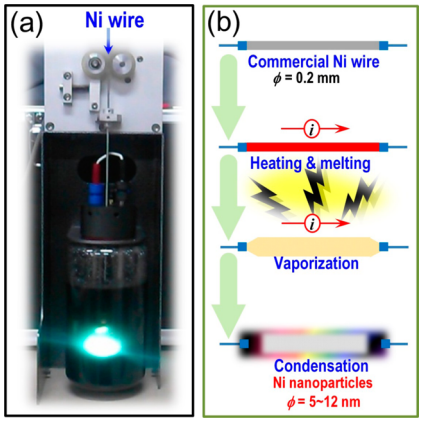

Figure 1. (a) Photographs showing the setup for the continuous electrical wire explosion process. (b) Schematic of working mechanism of the electrical wire explosion process.

process in OA. The Ni wire was continuously fed by a feeding roller installed between high-voltage electrodes within the exploding bottle. This setup enables simple production of nanocolloids and has the potential to be easily scaled-up. The working principle of the electrical wire explosion process is illustrated in Figure 1b. It is a pulse method where the nanoparticle is formed with each pulse. When a high rate of energy is injected by a pulse with high density current that passes through Ni wire, the Ni is superheated and evaporates with an explosion. The vapor is scattered at a high velocity into the surrounding liquid medium, OA. This explosive disintegration of the Ni wire is accompanied by a bright flash of light, as shown in Figure 1a. Subsequently, the condensed particles from the vapor cool quickly, which provides suitable conditions for synthesizing small Ni particles.[35−37]

Figure 2a shows the representative field-emission scanning electron microscopy (FESEM) images of the Ni nanopowders collected from the as-prepared Ni nanocolloids (Figure 2a inset, lower left) using the electrical wire explosion process, whence it is confirmed that uniform-sized Ni particles were produced. However, these nanoparticles showed a tendency to partially aggregate (Figure 2a inset, upper right).

All diffraction peaks in the X-ray diffraction (XRD) patterns of Ni nanopowders were perfectly matched to the Ni single phase (JCPDS card No. 04-0850). The partial thermochemical oxidation of as-prepared Ni nanopowders enabled the fabrication of uniform NiO/Ni nanopowders for conductive composite anodes. However, high oxidation temperatures led to significant decrease in the amount of metallic Ni, as shown in Figure S1 in the Supporting Information. Furthermore, the growth and coarsening of nanoparticles could be induced by the heat-treatment at high temperatures. After heat treatment at 300 °C in air, the XRD pattern partially changes and the resultant diffraction pattern represented NiO/Ni multiphases,

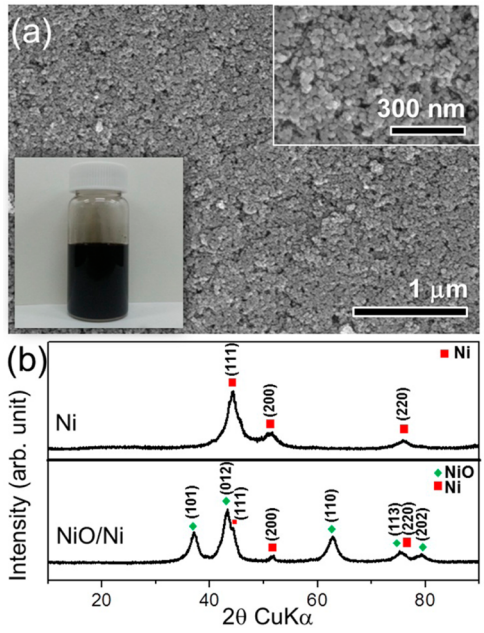

Figure 2. (a) Typical FESEM image of as-prepared Ni nanoparticles. Upper right and lower left insets show the magnified FESEM image of Ni nanoparticles and photograph of Ni colloids in OA, respectively. (b) XRD patterns of as-prepared Ni and NiO/Ni nanoparticles.

as can be seen in Figure 2b. The peaks of NiO at 37.25°, 43.29°, 62.85°, 75.4°, and 79.37° were attributed to diffraction from the (101), (012), (110), (113), and (202) planes and match the trigonal NiO structure (JCPDS card No. 44-1159). Furthermore, three minor peaks at 44.51°, 51.85°, and 76.37° indexed to the (111), (200), and (220) Ni planes, respectively, were also observed.

The specific surface area of the obtained Ni and NiO/Ni particles was determined by the nitrogen adsorption−desorption method. The curve of the nitrogen adsorption isotherm of IUPAC type IV is shown in Figure S2. Ni nanoparticles had a large Brunauer−Emmett−Teller (BET) surface area of 79.4 $m^2\ g^{-1}$. Although a slight growth in the nanoparticles was observed after partial oxidation at 300 °C (Figure S3), the BET surface area of NiO/Ni nanoparticles was estimated to be higher, approximately 93.0 $m^2\ g^{-1}$, which may be attributed the removal of surface organic residue.

The microstructures of the synthesized Ni and NiO/Ni powders were also characterized by transmission electron microscopy (TEM) and high-resolution TEM (HRTEM), as shown in Figure 3. Figure 3a shows a representative image of the as-prepared Ni nanoparticles, which revealed that most of the nanoparticles were spherical in shape with a diameter of about 5−12 nm. According to the selected area electron diffraction (SAED) pattern (Figure 3a inset), these nanoparticles were successfully indexed to the Ni phase. The HRTEM image of Ni nanoparticles are shown in Figure 3b, which reveals a *d*-spacing of 0.2 nm that corresponds to the (111) crystalline plane of Ni phase. NiO/Ni nanoparticles show similar spherical morphology with slightly larger particle size (Figure 3c). The SAED pattern (Figure 3c inset) revealed the formation of NiO/Ni composites. Based on the additional HRTEM analysis of NiO/Ni nanoparticles in Figure 3d, lattice spacing of 0.24 and 0.2 nm were indexed to the (101) plane of NiO and the (111) plane of Ni, respectively. No other phases

dx.doi.org/10.1021/am403643x | ACS Appl. Mater. Interfaces 2014, 6, 137−142

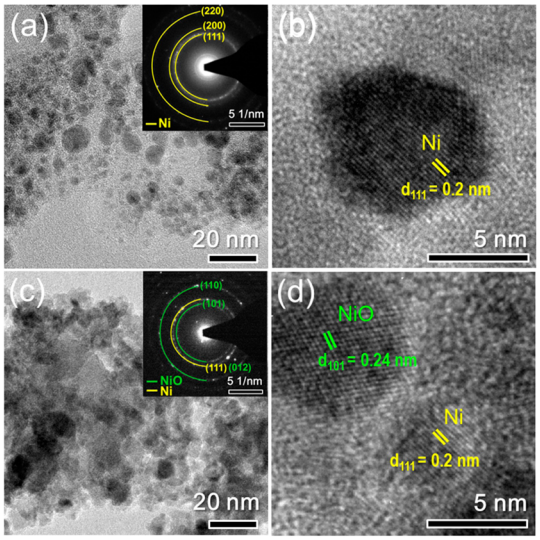

Figure 3. (a, b) TEM and HRTEM images of as-prepared Ni nanoparticles. (c, d) TEM and HRTEM images of as-prepared NiO/Ni nanoparticles. Insets of (a) and (c) show the SAED patterns of Ni and NiO/Ni nanoparticles, respectively.

can be observed in either the TEM or SAED patterns and these results were in agreement with the XRD analysis in Figure 2b.

The electrochemical property of NiO/Ni composites was analyzed by cyclic voltammetry (CV) and galvanostatic test. The CV curve obtained over a potential range from 0.01 to 3 V at a 0.3 mV s^{-1} scan rate for 10 cycles. As shown in Figure 4a, a

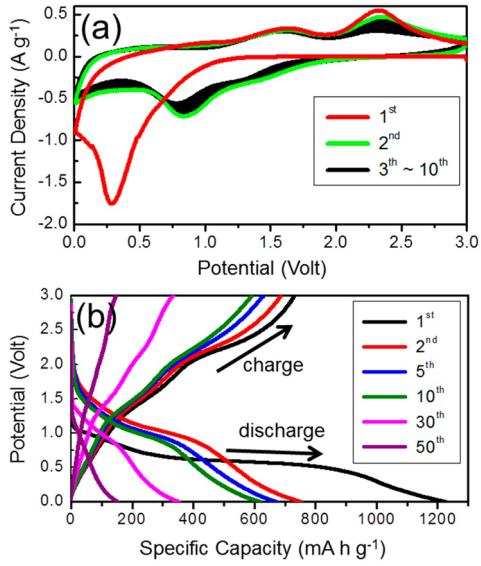

Figure 4. Typical (a) cyclic voltammograms and (b) charge−discharge curves of NiO/Ni nanoparticles.

strong peak was located near 0.25 V in the first cathodic scan that corresponds to the formation of a solid electrolyte layer (SEI) and the decomposition of NiO into Ni. During the first anodic scan, two peaks at around 1.5 and 2.2 V were observed. A weak peak near 1.5 V corresponds to the reoxidization of Ni to NiO and the decomposition of Li_2O matrix.[38,39] In the subsequent cycles, the cathode peaks shifts near 0.75 V because of a stable electrochemical reaction with lithium and surface texture changes due to the electrochemical reaction of Li^+ and NiO/Ni nanocomposites.

The galvanostatic cycling of NiO/Ni composites was carried out at a current density of 0.2 C (142 mA g^{-1}, based on the Li-conversion reaction of NiO, NiO + 2Li + $2e^- \rightarrow$ Ni + Li_2O).[8] Figure 4b displays the 1st, 2nd, fifth, 10th, 30th, and 50th charge/discharge profiles and reveals a larger first discharge capacity of 1226 mAhg^{-1} than the theoretical value (718 mA h g^{-1}). There is a rapid fall in the voltage to about 1 V after the first discharge with a long plateau around 0.75 V corresponding to the formation of the SEI layer and decomposition of NiO into Ni. The plateau during the charging cycle was located at about 1.5 and 2.25 V due to the reverse reaction of formation of NiO and these results correspond well with the CV data. The initial discharge and charge capacities were observed to be 1226 and 731 mA h g^{-1}, respectively. The reversible capacity of NiO/Ni showed large values, over 600 mA h g^{-1} but decreased to 148 mA h g^{-1} after 50 cycles, possibly due to the volume expansion of transition metal oxide anode materials during the repetitive charge/discharge cycles and aggregated particles present in the Ni composites.[40,41]

In order to overcome these drawbacks and to improve cycle performance of NiO/Ni, we synthesized NiO/Ni/graphene composites. To fabricate the NiO/Ni/graphene nanocomposites, we first investigated the dispersion behavior of commercially produced, graphenes, which have a thickness less than 1 nm and maximum x−y dimensions of 10 μm (Figure S4). A homogeneous graphene dispersion in OA was obtained by sonication. After suspending the graphenes, Ni/NiO nanoparticles were synthesized via electrical wire explosion process and subsequent partial oxidation at 300 °C, resulting in the formation of hybrid Ni/NiO/graphene nanocomposites.

Single particles or small clusters were observed without any appreciable agglomeration, as seen in typical TEM images of the NiO/Ni/graphene nanocomposites (Figure 5a, Supporting

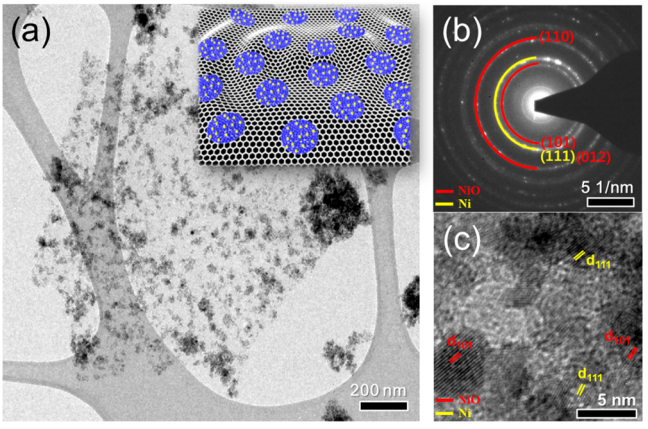

Figure 5. (a) TEM, (b) SAED, and (c) HRTEM images of NiO/Ni/graphene nanocomposites. Inset in (a) shows schematic illustration of NiO/Ni/graphene nanocomposites.

Information Figures S5 and S6). A simplified illustration of a NiO/Ni/graphene nanocomposite is provided in the inset of Figure 5a. Additionally, these nanoparticles were indexed as NiO and Ni having high crystallinity, based on the SAED pattern (Figure 5b) and HRTEM image (Figure 5c). The overall composition of NiO/Ni and NiO/Ni/graphene was evaluated using an electron probe microanalyzer (EPMA) by

dx.doi.org/10.1021/am403643x | ACS Appl. Mater. Interfaces 2014, 6, 137−142

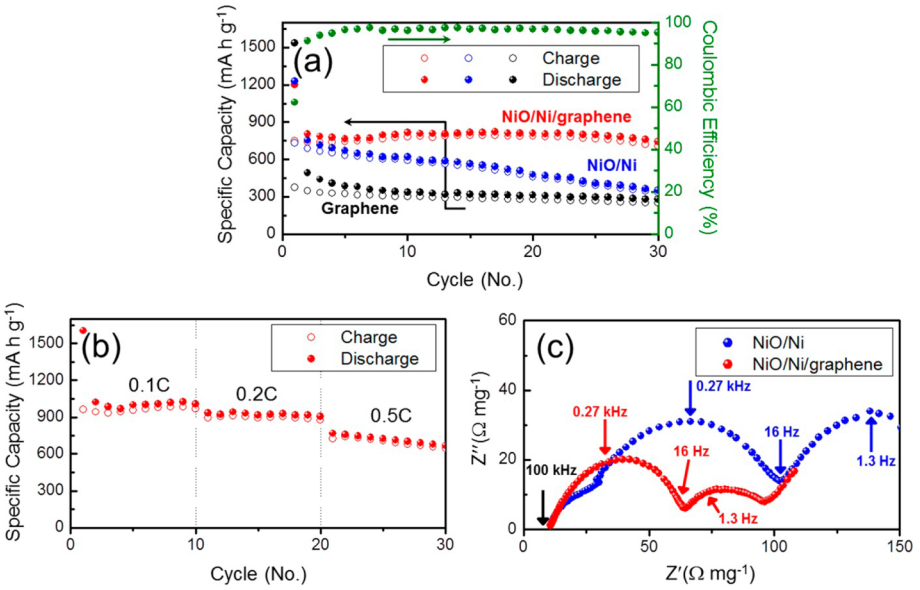

Figure 6. (a) Variation of the discharge−charge specific capacity with cycle number for NiO/Ni/graphene, NiO/Ni, and graphene electrodes. Coulombic efficiency of Ni/NiO/graphene electrode is also shown. (b) Rate capabilities for NiO/Ni/graphene electrodes at different C rate. (c) Typical impedance spectrum of NiO/Ni/graphene (red circle) and NiO/Ni (blue circle) electrode at 20th discharge state.

averaging at least 10 points for each sample. EPMA results indicated that 5 wt % of the graphene was incorporated in NiO/Ni/graphene nanocomposites. The metallic portion (NiO/Ni) in the composite can be easily adjusted by the control of graphene contents upon electrical wire explosion process. Additionally, the increase in number of pulses (3000 pulses in this work) led to the increase in the metallic portion in the composite because each pulse could generate the Ni nanocluster. Furthermore, the weight ratio of the NiO and Ni in these composites was 0.82:0.18 which is almost same ratio observed in NiO/Ni nanocomposites without graphene. In addition, the surface area of NiO/Ni/graphene nanocomposites increased to 137 m^2 g^{-1} due to the incorporation of graphenes with a much larger surface area.

The cyclability of the NiO/Ni/graphene electrodes cycled galvanostatically at a rate of 0.2 C (142 mA g^{-1}) is depicted in Figure 6a. For comparison, the variation in the discharge−charge capacity for NiO/Ni without graphene and pure graphene electrodes is also included in Figure 6a. Gradual capacity decay was observed in the NiO/Ni electrodes but the capacities of NiO/Ni/graphene electrodes stabilized around 700 mA h g^{-1}. This capacity value is much higher than the specific capacity of graphenes (Figure 6a) as well as conventional graphite electrodes. Furthermore, NiO/Ni/graphene electrodes exhibited Coulombic efficiency of 62% in the first cycle but very stable reversibility (Coulombic efficiency over 96%) was maintained after initial 5 cycles.

To demonstrate the rate capability of NiO/Ni/graphene electrodes, the cells were first cycled at a rate of 0.1 C and after every 10 cycles, the rate was increased in stages to 0.5 C (Figure 6b). NiO/Ni/graphene electrodes exhibited excellent rate performance, delivering charge capacities of ∼780, ∼700, and ∼500 mA h g^{-1} at rates of 0.1 C (71 mA g^{-1}), 0.2 C (142 mA g^{-1}), and 0.5 C (353 mA g^{-1}), respectively. The electrochemical performance of the NiO/Ni/graphene composite electrodes reported in this work is also superior to other reported NiO-based anodes.[42−44]

Electrochemical impedance spectroscopy (EIS) measurements were also carried out to compare the charge transfer resistances of the NiO/Ni and NiO/Ni/graphene electrodes. NiO/Ni/graphene electrodes deliver smaller diameters of both the high and low frequency semicircles after several cycles, indicating better electronic contact compared to NiO/Ni electrodes, as shown in Figure 6c. Therefore, graphenes with high conductivity can provide an efficient electron transport pathway from each active NiO nanoparticle to the current collector, thereby delivering reversible capacity and enhancing capacity retention and rate capability.

III. CONCLUSION

In summary, we have successfully synthesized NiO/Ni/graphene nanocomposites using a two-step route. First, we prepared a Ni/graphene precursor through a low-cost and highly scalable electrical wire explosion method using Ni wire in OA solvent medium containing graphenes. Subsequently, partial oxidation can produce NiO/Ni/graphene nanocomposites. The excellent cycle stabilities and rate capabilities of the NiO/Ni/graphene nanocomposite electrodes were proven to originate from the facile electronic delivery and the larger electrical contact area provided by the uniform distribution of NiO and Ni particles on graphenes without appreciable aggregation. We expect that this approach using the electrical wire explosion process will facilitate the fabrication of other nanocomposite electrodes with superior cycling performance.

IV. EXPERIMENTAL DETAILS

Synthesis of NiO/Ni/Graphene Nanococomposites. Commercial Ni wire (0.2 mm diameter) and graphene (ANGSTRON Materials) were used as precursors. Electrical pulse equipment (NTi-miniP, Nano Tech, Korea) was used to fabricate Ni nanoparticles. Electrical wire explosion was performed at 40 mm feeding distance and 320 V charging voltage in 700 mL OA with and without graphenes. Ni and Ni/graphene nanocolloids were sonicated and filtered through a Nylon membrane (Durapore, 0.22 mm, Millipore). The washing and filtering steps were performed several times using anhydrous ethanol and acetone. The nanoparticles were then dried in a vacuum oven at

dx.doi.org/10.1021/am403643x | ACS Appl. Mater. Interfaces 2014, 6, 137−142

70 °C for 5 h. For the partial oxidation, the resultant Ni and Ni/graphene nanopowders were heated in an alumina boat in a box furnace at 300 °C for 2 h in air.

Characterization. The morphology and crystal structure of the NiO/Ni and NiO/Ni/graphene composites were characterized by X-ray diffraction (XRD) (Miniflex II, Rigaku, Japan), field-emission scanning electron microscopy (FESEM) (JSM-6700F, JEOL, Tokyo, Japan), high-resolution transmission electron microscopy (HRTEM) (FEI, Tecnai G2 F30 S-Twin), and energy-dispersive X-ray spectroscopy (EDS). In addition, the specific surface areas of each powder were analyzed using the Brunauer−Emmett−Teller (BET, Belsor-mini II, BEL Japan) method with nitrogen adsorption−desorption. Quantitative elemental analyses were performed using an electron probe microanalyzer (EPMA-1600, Shimadzu, Japan).

Electrochemical Characterization. The electrochemical performance of the NiO/Ni and NiO/Ni/graphene nanocomposites was measured using Swagelok-type half-cells with Li metal foil as the negative electrode that was assembled in an argon-filled glovebox. Positive electrodes comprising the nanocomposite powders were cast on the Cu foil by mixing the prepared powders with Super P carbon black (MMM Carbon, Brussels, Belgium) as the conductive material and Kynar 2801 polymer binder (PVDF-HEP) at a mass ratio of 70:15:15 dissolved in 1-methyl-2-pyrrolidinone (NMP; Sigma-Aldrich). The slurry was spread onto the Cu foil and then dried in a vacuum oven at 100 °C for 4 h. Finally, half-cells were assembled using a separator film (Celgard 2400) saturated with a liquid electrolyte solution comprising 1 M $LiPF_6$ dissolved in ethylene carbonate (EC) and dimethyl carbonate (DMC) with volume ratio of 1:1. Assembled half-cells were evaluated using galvanostatic discharge/charge cycling under various current rates using a battery cycler (WBCS 3000, WonaTech) between 0.01 and 3 V. Electrochemical impedance measurement was performed using an electrochemical workstation (Ivium-n-Stat electrochemical analyzer, Ivium Technologies B. V., The Netherlands) over the range of 100 kHz to 10 mHz with an AC amplitude of 10 mV for 10 cycles.

■ ASSOCIATED CONTENT

Supporting Information

XRD patterns of as-prepared Ni and NiO/Ni nanoparticles heat-treated at various temperatures, nitrogen adsorption−desorption isotherms of as perpared Ni and NiO/Ni nanoparticles, typical FESEM images of NiO/Ni nanoparticles, TEM and HRTEM images of as-received graphenes, TEM image of NiO/Ni/graphene nanocomposites, EDS elemental mapping results for NiO/Ni/graphene nanocomposites. This material is available free of charge via the Internet at http://pubs.acs.org.

■ AUTHOR INFORMATION

Corresponding Author

*E-mail: dwkim@ajou.ac.kr.

Notes

The authors declare no competing financial interest.

■ ACKNOWLEDGMENTS

This research was supported by the National Research Foundation of Korea (NRF) funded by the Ministry of Science, ICT, and Future Planning (2012M1A2A2671802 and 2012R1A2A2A01 045382).

■ REFERENCES

(1) Kim, D. W.; Ko, Y. D.; Park, J. G.; Kim, B. K. *Angew. Chem., Int. Ed.* **2007**, *119*, 6744−6777.
(2) Guo, Y. G.; Hu, J. S.; Wan, L. J. *Adv. Mater.* **2008**, *20*, 2878−2887.
(3) Armand, M.; Tarascon, J. M. *Nature* **2008**, *451*, 652−657.
(4) Lee, C. W.; Seo, S. D.; Kim, D. W.; Park, S.; Jin, K.; Kim, D. W.; Hong, K. S. *Nano Res.* **2013**, *6*, 348−355.
(5) DiLeo, R. A.; Castiglia, A.; Ganter, M. J.; Rogers, R. E.; Cress, C. D.; Raffaelle, R. P.; Landi, B. J. *ACS Nano* **2010**, *4*, 6121−6131.
(6) Ko, Y. D.; Kang, J. G.; Lee, G. H.; Park, J. G.; Park, K. S.; Jin, Y. H.; Kim, D. W. *Nanoscale* **2011**, *3*, 3371−3375.
(7) Lee, G. H.; Sung, Y. M.; Park, J. G.; Chung, K. Y.; Cho, W. I.; Kim, D. W. *Nanotechnology* **2009**, *20*, 295205.
(8) Poizot, P.; Laruelle, S.; Grugeon, S.; Dupont, L.; Tarascon, J. M. *Nature* **2000**, *407*, 496−499.
(9) Li, Y.; Ten, B.; Wu, Y. *Nano Lett.* **2008**, *8*, 265−270.
(10) Mai, Y. J.; Tu, J. P.; Xia, X. H.; Gu, C. D.; Wang, X. L. *J. Power Sources* **2011**, *196*, 6388−6393.
(11) Yuan, Y. L. *J. Phys. Chem. C* **2010**, *114*, 2124−2126.
(12) Needham, S. A.; Wang, G. X.; Liu, H. K. *J. Power Sources* **2006**, *159*, 254−257.
(13) Zhou, G.; Wang, D. W.; Yin, L. C.; Li, N.; Li, F.; Cheng, H. M. *ACS Nano* **2012**, *6*, 3214−3223.
(14) Kottegoda, I. R. M.; Idris, N. H.; Lu, L.; Wang, J. Z.; Liu, H. K. *Electrochim. Acta* **2011**, *56*, 5815−5822.
(15) Parada, C.; Moran, E. *Chem. Mater.* **2006**, *18*, 2719−2725.
(16) Wang, W.; Liu, Y.; Xu, C.; Zheng, C.; Wang, G. *Chem. Phys. Lett.* **2002**, *362*, 119−122.
(17) Sietsma, J. R. A.; Meeldijk, J. D.; Breejen, J. P. D.; Helder, M. V.; Dillen, A. J. V.; Jongh, P. E. D.; Jong, K. P. D. *Angew. Chem., Int. Ed.* **2007**, *46*, 4547−4549.
(18) Kung, D. B.; Lei, B. X.; Pan, Y. P.; Yu, X.; Su, C. Y. *J. Phys. Chem. C* **2009**, *113*, 5508−5513.
(19) Yang, Q.; Sha, J.; Ma, X.; Yang, D. *Mater. Lett.* **2005**, *59*, 1967−1970.
(20) Reddy, A. L. M.; Gowda, S. R.; Shaijumon, M. M.; Ajayan, P. M. *Adv. Mater.* **2012**, *24*, 5045−5064.
(21) Wang, W.; Kumta, P. N. *ACS Nano* **2010**, *4*, 2233−2241.
(22) Gao, Q.; Yang, L.; Lu, X.; Mao, J.; Zhang, Y.; Wu, Y.; Tang, Y. *J. Mater. Chem.* **2010**, *20*, 2807−2812.
(23) Kim, H. Y.; Seo, D. W.; Kim, S. W.; Kim, J. S.; Kang, K. S. *Carbon* **2011**, *49*, 326−332.
(24) Zhang, W. D.; Xu, B.; Jiang, L. C. *J. Mater. Chem.* **2010**, *20*, 6383−6391.
(25) Du, N.; Zhang, H.; Chen, B.; Wu, J.; Ma, X.; Liu, Z.; Zhang, Y.; Yang, D.; Huang, X.; Tu, J. *Adv. Mater.* **2007**, *19*, 4505−4509.
(26) Ding, S.; Chen, J. S.; Lou, X. W. *Adv. Funct. Mater.* **2011**, *21*, 4120−4125.
(27) Hwang, I. S.; Kim, J. C.; Seo, S. D.; Lee, S.; Lee, J. H.; Kim, D. W. *Chem. Commun.* **2012**, *48*, 7061−7063.
(28) Lou, X. W.; Deng, D.; Lee, J. Y.; Archer, L. A. *Chem. Mater.* **2008**, *20*, 6562−6566.
(29) Xiang, H. F.; Li, Z. D.; Xie, K.; Jiang, J. Z.; Chen, J. J.; Lian, P. C.; Wu, J. S.; Yu, Y.; Wang, H. H. *RSC Adv.* **2012**, *2*, 6792−6799.
(30) Hou, J.; Shao, Y.; Ellis, M. W.; Moore, R. B.; Yi, B. *Phys. Chem. Chem. Phys.* **2011**, *13*, 15384−15402.
(31) Dai, L. *Acc. Chem. Res.* **2013**, *46*, 31−42.
(32) Tao, L.; Zai, J.; Wang, K.; Wan, Y.; Zhang, H.; Yu, C.; Xiao, Y.; Qian, X. *RSC Adv.* **2012**, *2*, 3410−3415.
(33) Zou, Y.; Wang, Y. *Nanoscale* **2011**, *3*, 2615−2620.
(34) Zhu, X. J.; Hu, J.; Dai, H. L.; Ding, L.; Jiang, L. *Electrochim. Acta* **2012**, *64*, 23−28.
(35) Kotov, Y. A. *J. Nanopart. Res.* **2003**, *5*, 539−550.
(36) Kotov, Y. A. *Nanotechnol. Russ.* **2009**, *4*, 415−424.
(37) Sedoi, V. S.; Ivanov, Y. F. *Nanotechnology* **2008**, *19*, 145710.
(38) Zhang, G.; Chen, Y.; Qu, B.; Hu, L.; Mei, L.; Lei, D.; Li, Q.; Chen, L.; Li, Q.; Wang, T. *Electrochim. Acta* **2012**, *80*, 140−147.
(39) Debart, A.; Dupont, L.; Poizot, P.; Leriche, J. B.; Tarascon, J. M. *J. Electrochem. Soc.* **2001**, *148*, A1266−A1274.
(40) Ma, J.; Yang, J.; Jiao, L.; Mao, Y.; Wang, T.; Duan, X.; Lian, J.; Zheng, W. *CrystEngComm* **2012**, *14*, 453−459.
(41) Liu, L.; Li, Y.; Yuan, S.; Ge, M.; Ren, M.; Sun, C.; Zhou, Z. *J. Phys. Chem. C* **2010**, *114*, 251−255.

(42) Xie, D.; Yuan, W.; Dong, Z.; Su, Q.; Zhang, J.; Du, G. *Eletrochim. Acta* **2013**, *92*, 87−92.
(43) Yuan, L.; Guo, Z. P.; Konstantinov, K.; Munroe, P.; Liu, H. K. *Electrochem. Solid-State Lett.* **2006**, *9*, A524−A528.
(44) Li, X.; Dhanabalan, A.; Wang, C. *J. Power Sources* **2011**, *196*, 9625−9630.